Proceedings of the 26th International Conference on
Port and Ocean Engineering under Arctic Conditions
June 14-18, 2021, Moscow, Russia

Breakage of saline ice blocks in ice-to-ice contact

Malith Prasanna[1], Mingdong Wei[1], Arttu Polojärvi[1], David M. Cole[2]
[1]Aalto University, School of Engineering, Department of Mechanical Engineering, P.O. Box 14100, FI-00076 Aalto, Finland
[2]ERDC-CRREL (Ret.), 72 Lyme Rd., Hanover, NH 03768, USA

ABSTRACT

This paper focuses on the experiments on breakage of laboratory grown floating saline ice blocks in ice-to-ice contact. Insight on breakage is required in modeling force transmission through an ice rubble pile, since it occurs through so-called force chains, which may collapse due to buckling or the failure of individual ice blocks within the chain. In the experiments, 300 × 300 × 110 mm^3 ice blocks were set to float, brought into contact to form ice-to-ice contacts, and compressed up to failure. The force transmitted through the contacts and the failure process were recorded. It was concluded that the shear-like failure of the blocks limited the contact forces, as it occurred in about 75% of the 32 experiments performed.

KEY WORDS: Ice mechanics; Breakage mechanism; Force chain; Shear failure

INTRODUCTION

Peak ice load events on offshore structures occur during complex ice-structure interaction processes (Daley et al., 1998). One important mechanism behind them are force chains; a series of ice blocks in contact with each other and the structure under high compressive stress. Magnitudes of the peak loads are limited by the failure of force chains, which may occur due to the buckling of the chain or local failure at the block-to-block contacts (Paavilainen and Tuhkuri, 2013; Ranta et al., 2018; Ranta and Polojärvi, 2019). Local failures were visually observed to occur in direct shear box experiments, where maximum loads were related to force chains (Polojärvi et al., 2015; Pustogvar et al., 2014). In discrete element method simulations of ice-structure interactions, the local failure at contact is often accounted for by choosing the upper limit of the contact pressure as the compressive strength of ice (Hopkins, 1992; Paavilainen et al., 2009; Tuhkuri and Polojärvi, 2018; van den Berg et al., 2018). However, there are no experimental data justifying this choice of parameterization, which motivates the experiments described here.

Here we focus on laboratory-scale experiments on ice block breakage performed using an experimental set-up allowing testing of laboratory-grown saline, floating ice blocks with a naturally occurring temperature gradient. The objective was to generate data on ice block breakage under ice-to-ice contact forces by using a simple contact geometry. This is important for describing the limit mechanisms for ice loads and in developing numerical models for sea ice loading; what limits the load that the ice blocks compressed together may transmit? The experiments were performed in the cold room of the Department of Mechanical Engineering, Aalto University. The present paper summarizes the findings presented in Prasanna et al. (2021).

EXPERIMENTS

The ice growing tank, the ice growing procedure and the testing rig used are described in detail by Wei et al. (2020). Figure 1a illustrates the breakage experiments. The three-block system used was designed to model the type of contacts that would have the maximum force carrying capacity within a force chain. Ice blocks used in the experiments were laboratory-grown, saline ice specimens with nominal dimensions of 300 mm × 300 mm × 110 mm (width × length × thickness). The laboratory ice had S2 columnar grain structure and the grain size was approximately 3 mm. The density and the salinity of the ice were 886 kg m^{-3} and 5 ppt, respectively.

The testing rig used was a closed-loop, force-controlled uniaxial hydraulic compression press mounted in a saline water basin. Figure 1b shows the testing rig with the ice specimens set up for a test. The rig consisted of three sets of load cells to measure the piston force and reaction forces, and a displacement gauge to measure the piston displacement. The saline water in the test basin was from the ice growing tank transferred immediately before harvesting the ice specimens. Thus, the water temperature and salinity in the test basin were virtually the same as in the ice growing tank. Once harvested from the ice growing tank, specimens were moved to the test basin quickly and set to float with no significant temperature change or brine drainage.

The average temperature of the floating ice specimens was -2.5℃ and was stable within the duration of the experiments. The air temperature of the cold room was -10°C throughout the experiments.

In the experiments, three specimens were brought into contact to form two ice-to-ice contacts as shown in Figure 1a and compressed at a rate of 5 kNs^{-1} until the ice specimens failed. The loading rate here was chosen so that the experiments would be long enough to study the progressive failure of the three-block system without any significant creep in the specimens. The compressive force applied by the hydraulic piston, F_p, and reaction forces F_1 and F_2 were recorded. F_1 and F_2 were equal to the forces transmitted by the two ice-to-ice contacts. Thirty-two experiments were conducted using six contact lengths, as presented in

Table 1.

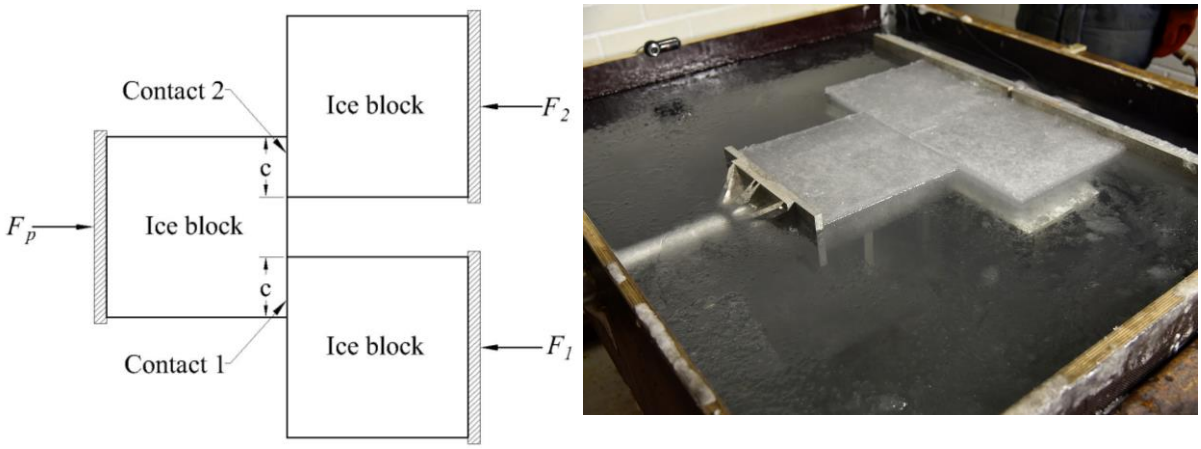

a) b)

Figure 1. (a) Illustration of the three-block system showing two contacts of length c, the piston force, F_p, and the reaction forces F_1 and F_2 and (b) photo of the experimental set-up. Figure (a) reproduced from Prasanna et al. (2021).

Table 1. Experiment matrix. In the table, 'contact area' is the total area of two contacts (2×c×ice thickness, where c is the contact length).

c [mm]	Contact area [m^2]	Number of experiments
25	0.005	4
50	0.010	4
75	0.015	5
100	0.020	8
125	0.025	5
150	0.030	6

RESULTS

Typical piston force-displacement (F_p-d) curve from an experiment with contact length c = 50 mm is presented in Figure 2a. As the figure shows, F_p-d records has a linear portion with nonlinear parts at the start and near the peak. Blocks settling at their contacts caused the nonlinearity at the beginning of the experiment. The nonlinear behavior close to the peak was due to the formation of microcracks and inelastic deformations on the failure planes, indicating the quasi-brittle characteristics of the failures. The steep drop in the F_p-d curve was due to the failure of the ice blocks. The second peak in the F_p-d curve was due to the failure of the second contact, which did not have any effect on the initial ice failure at the contacts.

F-t records of the same experiment are presented in Figure 2b. The figure shows compressive force, F_p as well as the force transmitted by the two contacts, F_1 and F_2 (Figure 1a). As the figure indicates, failure first occurred at one of the contacts followed by the immediate failure of the second contact as total F_p, became transmitted by it. The analysis was focused on the first contact that failed as the loading on the three-block system became asymmetric after the first failure. The maximum force transmitted by the first contact to fail, max(F_c), was defined as the failure force of the contact. As expected, max(F_c) increased with the length of the contact.

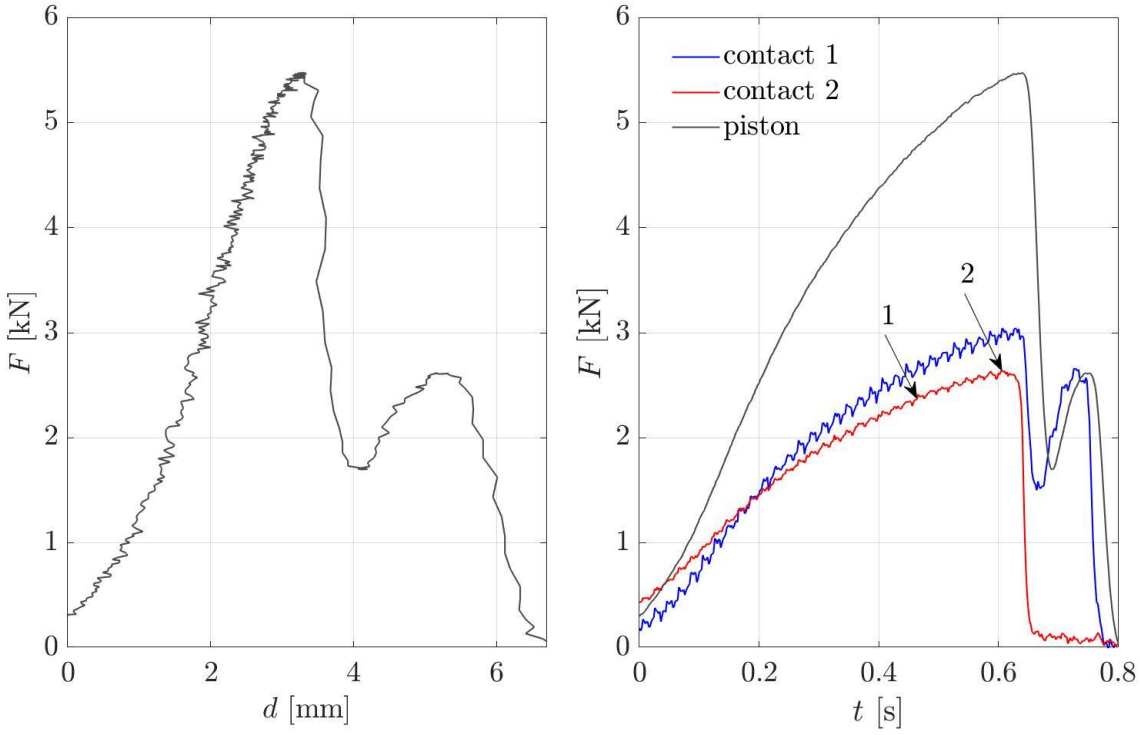

Figure 2. Typical F_p-d and F-t curves for contact lengths c=50 mm. Markers 1 and 2 in figure (b) indicate time instances with 90% of maximum contact force and max(F_c), respectively. Figure 3 shows snapshots of the experiment from time instances 1 and 2.

Figure 3 presents four-photo sequence of the contact failure from the experiment with its force records presented in Figure 2. The first two photos of the sequence correspond to the time instances, 90% and 100% of max(F_c), as indicated in Figure 2b, and the final two photos correspond to the first and the second failure of contacts. Figure 3b and 3c show the material damage appearing as white bands on the areas of the final failure planes before the failure of the contacts. The white bands were due to the incremental material damage accumulating along the subsequent final failure planes and were observed in all the experiments. The nonlinearity close to the peak of the F_p-d curve was caused by the damaged material accumulating along the eventual failure planes. Similar bands of material, showing incremental damage before the failure, were observed in all experiments. The shear-like failure process at the contacts presented in the Figure 3 was observed consistently in all the experiments with failures occurring in all three blocks. The angle between the loading direction and the failure planes varied from about 15° to 30°. Moreover, the max(F_c) was proportional to the length of these shear bands as discussed in the next section. Thus, the failures observed here can be characterized as material failure due to the lack of strength rather than instantaneous crack propagation.

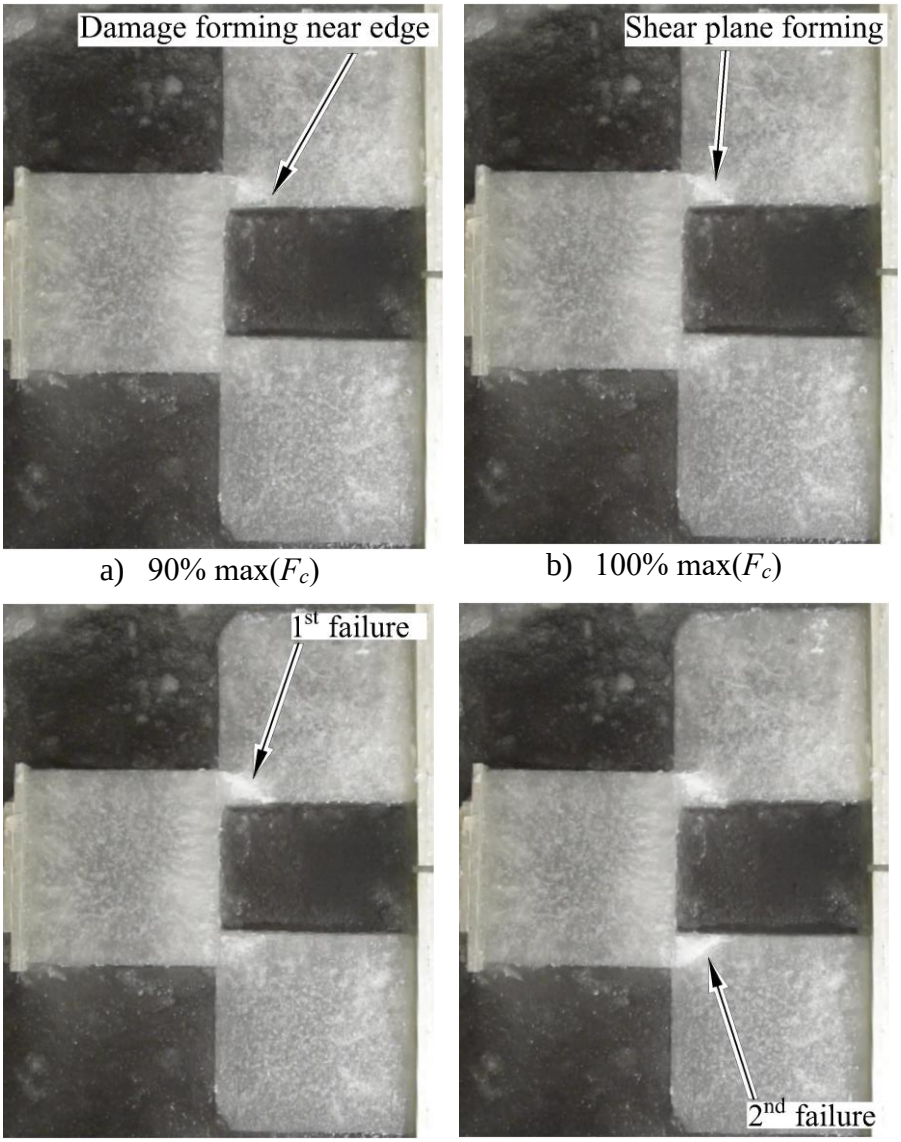

a) 90% max(F_c) b) 100% max(F_c)

c) Instance of first failure d) Instance of second failure

Figure 3. Failure process of the c=50 mm experiment. Figure reproduced from Prasanna et al. (2021).

ANALYSIS

Failure in Figure 3 can be characterized as 'Coulombic shear faults', a common failure mechanism of ice under low axial confinement (Golding et al., 2010). These faults were characterized by failure planes formed of interconnected microcracks and had about 20° to 30° angle with respect to the principal stress direction. The critical shear force resolved on the failure plane can be calculated as presented in Figure 4. At the instance of max(F_c), the quasi-static force equilibrium at the shear plane yields equations,

$$F_\tau = \max(F_c) \cdot \cos(\theta)\,, \tag{1}$$

$$F_n = \max(F_c) \cdot \sin(\theta)\,, \tag{2}$$

where F_τ and F_n are the critical shear and normal force resultants aligning with and perpendicular to the shear plane having an angle θ, respectively. Therefore, for the shear-like failures, F_τ can be calculated using max(F_c) and θ from the experiments. Here the θ was obtained by first tracing the failure plane using the images from the experiments, and then by using MATLAB to fit a line along the failure plane. Moreover, the area of the failure plane $A\tau$ can also be estimated using the length of the failure plane and the ice thickness.

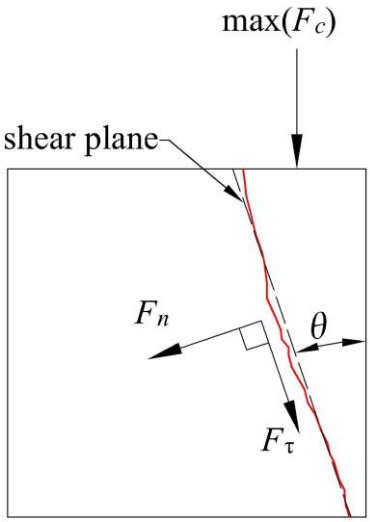

Figure 4. Normal and shear forces resolved on the failure plane for quasi-static force equilibrium at the critical moment of shear failure. max(F_c) is the maximum contact force. F_τ and F_n are shear and normal forces along the failure plane, respectively. θ is the failure angle. Figure reproduced from Prasanna et al. (2021).

Figure 5 reports the calculated $F\tau$ values plotted against $A\tau$ for shear-like failures. In addition to the data points, the figure shows a linear fit for the data. The fit has a coefficient of determination, R^2=0.73 and a physically-sound zero intercept which suggests that the curve adequately represents the experimental results. Importantly, the linear fit also implies that the maximum contact force was limited by the shear strength of the ice and the slope of the fit, 279 kPa, can be interpreted to present the shear strength of the ice specimens used in the experiments.

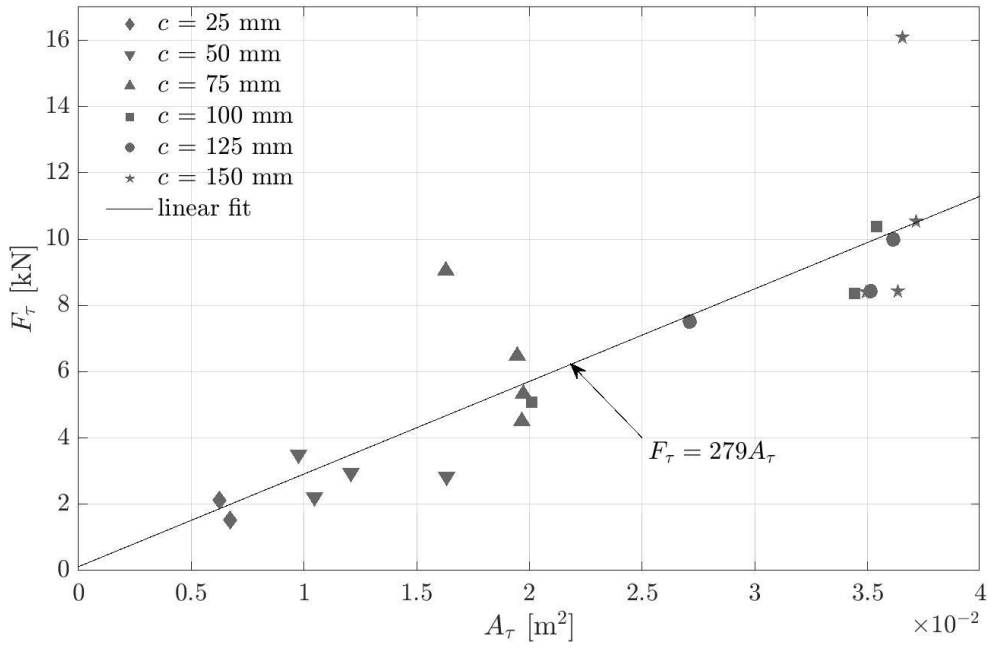

Figure 5. Critical shear force F_τ vs. failure plane area A_τ. The coefficient of determination for the linear fit was R^2=0.73. Figure reproduced from Prasanna et al. (2021).

The present results have implications on numerical modeling of ice-structure interaction processes. As mentioned above, discrete element simulations are popular tools in ice mechanics. In such simulations, simplified contact force models are typically used and it has been common to choose the upper limit for the maximum contact force based on the contact area and the compressive or crushing strength of ice (Hopkins, 1992; Paavilainen et al., 2009; Paavilainen and Tuhkuri, 2013; Ranta and Polojärvi, 2019; van den Berg et al., 2018). However, results of this study suggest that crushing failure at the contact may often not be the plausible failure mode of the contact, but shear-like failure of the ice blocks has to be considered as well. It is worth highlighting that the choice of the load-limiting parameter will depend on the assumed ice failure mode, and not all of these modes are explored here.

CONCLUSIONS

Laboratory experiments on ice block breakage under ice-to-ice contacts were conducted using laboratory-grown, saline ice specimens with an unaligned columnar microstructure. The objective of the experiments was to investigate the ice block breakage with regards to the force transmission in ice rubble piles. The primary mode of failure for the ice blocks in ice-to-ice contact was shear. Failure planes observed in the experiments had the characteristics of 'Coulombic shear faults'. This failure mechanism should be accounted for in numerical modeling of ice structure interaction processes and in ice load models related to force chains. The experiments and their results are presented in detail in Prasanna et al. (2021).

ACKNOWLEDGEMENTS

The authors are grateful for the financial support from the Academy of Finland through the pr oject (309830) Ice Block Breakage: Experiments and Simulations (ICEBES).

REFERENCES

Daley, C., Tuhkuri, J., Riska, K., 1998. The role of discrete failures in local ice loads. *Cold Regions Science and Technology* 27, 197–211.

Golding, N., Schulson, E.M., Renshaw, C.E., 2010. Shear faulting and localized heating in ice: The influence of confinement. *Acta Materialia* 58, 5043–5056.

Hopkins, M.A., 1992. *Numerical simulation of systems of multitudinous polygonal blocks*. Cold Regions Research and Engineering Laboratory (US) Report 92-22, 69p.

Paavilainen, J., Tuhkuri, J., 2013. Pressure distributions and force chains during simulated ice rubbling against sloped structures. *Cold Regions Science and Technology* 85, 157–174.

Paavilainen, J., Tuhkuri, J., Polojärvi, A., 2009. 2D combined finite-discrete element method to model multi-fracture of beam structures. *Engineering Computations* (Swansea, Wales) 26, 578–598.

Polojärvi, A., Tuhkuri, J., Pustogvar, A., 2015. DEM simulations of direct shear box experiments of ice rubble: Force chains and peak loads. *Cold Regions Science and Technology* 116, 12–23.

Prasanna, M., Wei, M., Polojärvi, A., Cole, D.M., 2021. Laboratory experiments on floating saline ice block breakage in ice-to-ice contact. *Cold Regions Science and Technology* (in press)

Pustogvar, A., Polojärvi, A., Høyland, K.V., Bueide, I.M., 2014. Laboratory scale direct shear box experiments on ice rubble: The effect of block to box size ratio, in: *Proceedings of the International Conference on Offshore Mechanics and Arctic Engineering - OMAE*.

Ranta, J., Polojärvi, A., 2019. Limit mechanisms for ice loads on inclined structures: Local crushing. *Marine Structures* 67.

Ranta, J., Polojärvi, A., Tuhkuri, J., 2018. Limit mechanisms for ice loads on inclined structures: Buckling. *Cold Regions Science and Technology* 147, 34–44.

Tuhkuri, J., Polojärvi, A., 2018. A review of discrete element simulation of ice-structure interaction. *Philosophical Transactions of the Royal Society A: Mathematical, Physical and Engineering Sciences* 376.

van den Berg, M., Lubbad, R., Løset, S., 2018. An implicit time-stepping scheme and an improved contact model for ice-structure interaction simulations. *Cold Regions Science and Technology* 155, 193–213.

Wei, M., Polojärvi, A., Cole, D.M., Prasanna, M., 2020. Strain response and energy dissipation of floating saline ice under cyclic compressive stress. *The Cryosphere* 14, 2849–2867.